Research Paper

# Gravity Data Decomposition through Upward Continuation and Wavelet Transform, Case Study at Muria Peninsula, Java Island, Indonesia

**Adelia Nanda Pramudya[1], Rina Dwi Indriana[2], La Ode M Sabri[3], Arisuna Maulidyan Pahlevi[4]**

[1]Post Graduate Student, Physics Department, Faculty of Science and Mathematics, Diponegoro University, Semarang, Indonesia,
[2]Physics Department, Faculty of Science and Mathematics, Diponegoro University, Semarang, Indonesia,
[3]Geodetic Engineering Department, Faculty of Engineering, Diponegoro University, Semarang, Indonesia,
[4]Center for Geodetic Control Network and Geodynamica, Geospatial Information Agency, Bogor, Indonesia.

Corresponding Author: Rina Dwi Indriana

## ABSTRACT

The separation of regional and residual anomalies is a challenge in gravity data analysis. This study offers a new perspective by comparing gravity anomaly separation using the upward continuation method and wavelet transformation. This study uses airborne gravity measurements from the Indonesian Geospatial Information Agency survey in the Muria Peninsula. Airborne gravity data in the form of Free Air Anomaly (FAA) is corrected for Bouguer and terrain effects to produce the Complete Bouguer Anomaly (CBA). The CBA is then processed using both upward continuation and wavelet transformation to obtain regional and residual anomalies. The results show that regional and residual anomalies derived from the upward continuation and wavelet transformation methods yield similar values. Regional anomalies range from 17 to 38 mGal, while residual anomalies range from -85 to 35 mGal. The regional anomaly obtained through wavelet transformation successfully detects deeper anomalous sources, particularly the magma conduit between Mount Muria and Mount Genuk. Residual anomalies identified using wavelet transformation reveal shallow anomalous structures, including calderas and maars around Mount Muria, the Patiayam Formation at Mount Genuk, and local faults in the Rembang Fold Zone.

*Keywords:* Gravity airborne, regional and residual anomaly, upward continuation, wavelet transform, Muria Peninsula

## INTRODUCTION

Various geophysical methods are used to study the earth's subsurface structure, one of which is the gravity method. This method is considered one of the most effective techniques for identifying density variations in the earth's subsurface [1,2]. Initially, gravity measurements relied on conventional single-pendulum methods, which were relatively complex [3,4]. Over time, modern techniques using gravimeters and satellites have been developed [5]. However, land-based gravimeter surveys can be time-consuming, and satellite-based measurements rely on mathematical models of the Earth, resulting in lower data resolution. A more effective approach is airborne gravity, which involves measurements taken from an aircraft. Airborne gravity allows for rapid data acquisition over large areas and facilitates

surveys in regions with challenging topography and terrain [6].

The measurement of earth's gravity field presents a unique challenge, as the readings encompass all field sources, from shallow basement rocks to the deeper mantle [7]. The response of field sources at various depths correlates with wavelength. Longer wavelengths correspond to deeper field sources, while shorter wavelengths indicate shallower sources [8,9]. In some cases, long-wavelength field sources are utilized for regional studies, such as Moho depth investigations [10-12]. Conversely, short-wavelength field sources are used to analyze shallow residual structures, such as basement lithology [13,14]. Thus, the terms regional and residual gravity fields refer to two distinct field sources, depending on the study's scope.

Regional and residual field sources can be separated using various methods to facilitate interpretation [15]. Some commonly used methods include upward continuation, polynomial fitting, trend surface analysis, and moving average filtering [16-19]. These methods are based on filtering processes and are often used due to their practicality and simplicity. Another method that is still rarely applied to gravity data is wavelet transform. This study provides a comparative analysis between the upward continuation method and wavelet transform and applies these techniques to evaluate Bouguer anomalies in the Muria Peninsula. The findings of this study present new insights into Bouguer anomalies based on airborne gravity data in the Muria Peninsula, which have not been explored before.

## MATERIALS & METHODS
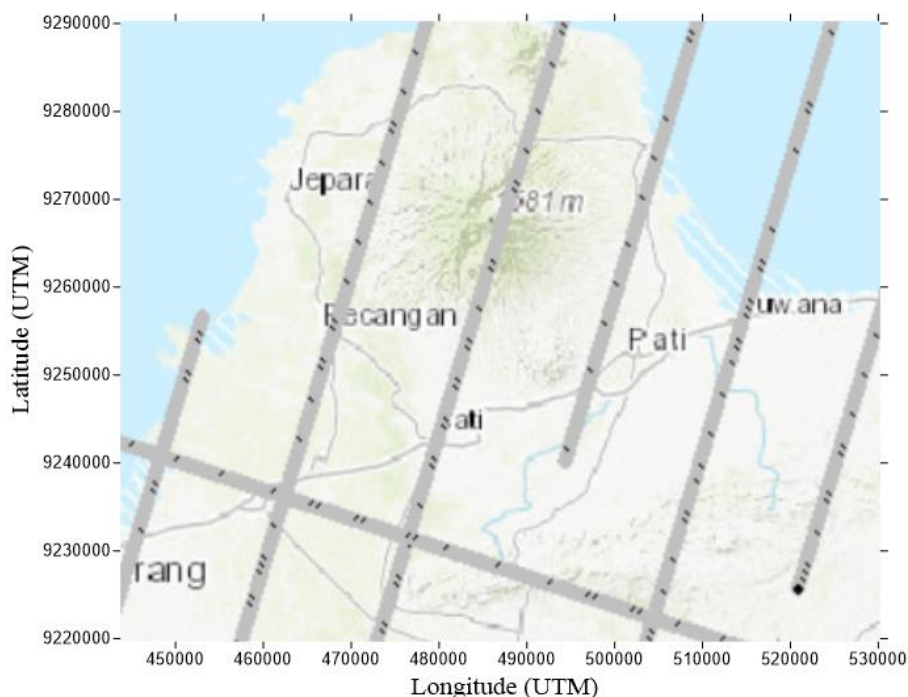### Airborne Gravity Survey



**Figure 1. Airborne gravity survey lines in the Muria Peninsula Area**

This research utilizes airborne gravity data and DEM data. The airborne gravity data were collected in 2019 through a joint project between the Indonesian Geospatial Information Agency and National Chiao Tung University. Data acquisition was conducted using an aircraft equipped with a GPS Aerocontrol IIb at an average altitude of 4 km above sea level. The airborne gravity data include coordinate data, free-air anomaly (FAA), ellipsoidal height, and orthometric height. The DEM data used in this study is the SRTM DEM with a 30 m grid resolution. Both datasets cover the entire

study area, which spans $86\,\text{km} \times 70\,\text{km}$ in the Muria Peninsula region.

As shown in Figure 1, the flight path was at an altitude of 4 km, requiring reduction to minimize noise caused by aircraft movement. Equation (1) represents the principle of airborne gravity measurements [20].

$$\vec{g}_z = (\vec{f}_z - \vec{f}_b) - \ddot{u} + \vec{g}_0 \left[ 2\vec{w}_e \cos\varphi + \frac{\vec{v_e}}{(R_N+z)} \right]\vec{v_e} + \frac{\vec{v_n^2}}{(R_M+z)} \qquad (1)$$

Equation (1) explains that gravimeter readings at altitude z are $\vec{f}_z$ dan $\vec{f}_b$, while the last two terms represent the effect of gravity variations due to changes in centrifugal acceleration caused by velocity direction changes (eotvos effect). Components such as $z, \ddot{u}, v_{e,} v_{n,} \varphi$ are obtained through GPS and IMU. Additional reductions, such as downward continuation, are also applied to obtain gravity values at geoid height. Gravity data reduction, including Bouguer and terrain corrections, is implemented to derive the CBA, which is mathematically represented in Equation (2) [21].

$$\Delta g_{BL} = g_{obs} - (g_n - FA + B - T) \qquad (2)$$

$\Delta g_{BL}$ represents the CBA, $g_{OBS}$ is the gravity observation, $g_n$ is the normal gravity, FA is the free air anomaly, B is the Bouguer correction, and T is the terrain correction. CBA is a superimposed dataset consisting of regional and residual anomalies. The regional and residual data are obtained through filtering methods, namely upward continuation and wavelet transformation.

## Upward Continuation

Upward continuation is a mathematical technique used to separate shallow gravity anomaly sources from deeper sources. It calculates anomaly values at a point below the surface, at the mean sea level, and at a height h above the surface. The gravitational attraction caused by a mass element (dm) at coordinates $(x_0, y_0, z_0)$ at a distance R (x, y, z) is expressed in Equation (3) [22].

$$dg = \frac{Gdm}{R^2} = \frac{Gdm}{(x-x_0)^2+(y-y_0)^2+(z-z_0)^2} \qquad (3)$$

The vertical anomaly $dg_z$ contributes to the source at the mean sea level point, as shown in Equation (4).

$$dg_z = \Delta g_0 = \frac{Gdm}{R^2}\frac{z}{R} = Gdm\frac{z}{R^3} = Gdm\frac{z}{[(x-x_0)^2+(y-y_0)^2+z^2]^{3/2}} \qquad (4)$$

Therefore, the projection of the anomaly at a height h above sea level is expressed in Equation (5).

$$\Delta g_p = \frac{Gdm}{S^2}\frac{z+h}{S} = Gdm\frac{(z+h)}{S^3} = Gdm\frac{(z+h)}{[(x-x_0)^2+(y-y_0)^2+(z+h)^2]^{3/2}} \qquad (5)$$

Equation (5) expresses the gravitational attraction caused by a mass element (dm) beneath the surface at $(x_0, y_0, z_0)$ at a height h above sea level. The upward continuation method can directly separate anomaly sources with long and short wavelengths [23].

## Wavelet Transform

Wavelet transform can be considered an extension of the Fourier transform. While the Fourier transform provides frequency resolution, the wavelet transform offers both frequency and time resolution. The ability to analyze data in greater detail using wavelet transform is known as multiresolution analysis. The wavelet transform can provide detailed local signal results according to the desired frequency. Another advantage of the wavelet transform is its ability to analyze non-stationary signals, making it an effective tool for geophysical data analysis. Physical phenomena can be processed into more recognizable objects, smoothed objects, and compressed objects [24].

There are two types of wavelet transform, Discrete Wavelet Transform (DWT) and Continuous Wavelet Transform (CWT). DWT is more commonly used in research as it requires less processing time. DWT separates signals into high-frequency and low-frequency components. The fundamental function of DWT is mathematically expressed in Equation (6) [25].

$$\Psi_{a,b}(t) = \frac{1}{\sqrt{a}}\Psi\left(\frac{t-a}{a}\right) a,b \in R, a > 0 \qquad (6)$$

With a and b representing the scale and shift factors, respectively [26]. High frequencies

are obtained using a high-pass filter, while low frequencies are obtained using a low-pass filter. This process is known as signal decomposition, which is mathematically expressed in Equation (7).

$$\Delta \vec{g}(x,y) = A_p f(x,y) + \sum_{j=1}^{p} \sum_{\varepsilon=1}^{3} D_j^{\varepsilon} f(x,y) \quad (7)$$

With $\Delta g(x,y)$ representing the complete Bouguer anomaly, $p$ denoting the order of the wavelet, $A_p f(x,y)$ as the approximation field of order $p$ obtained from the low-pass filter, and $D_j^{\varepsilon} f(x,y)$ as the detail field of order $p$ obtained from the high-pass filter. After the signal is decomposed, thresholding is applied to determine the threshold value based on the rule given in Equation (8).

$$Y_{hard} = \begin{cases} \omega_i | \omega_i| \geq \lambda \\ 0 | \omega_i| < \lambda \end{cases}$$

$$Y_{soft} = \begin{cases} sgn(\omega_i) * (|\omega_i| - \lambda) | \omega_i| \geq \lambda \\ 0 | \omega_i| < \lambda \end{cases} \quad (8)$$

The threshold can be set as a hard or soft function. The hard threshold function sets the signal to zero if its value is below the specified threshold. The soft threshold function sets the signal to zero and reduces the signal if its value exceeds the specified threshold. The final phase in wavelet transform for anomaly separation is reconstruction. Reconstruction can utilize detail coefficients from level 1 to N [25].
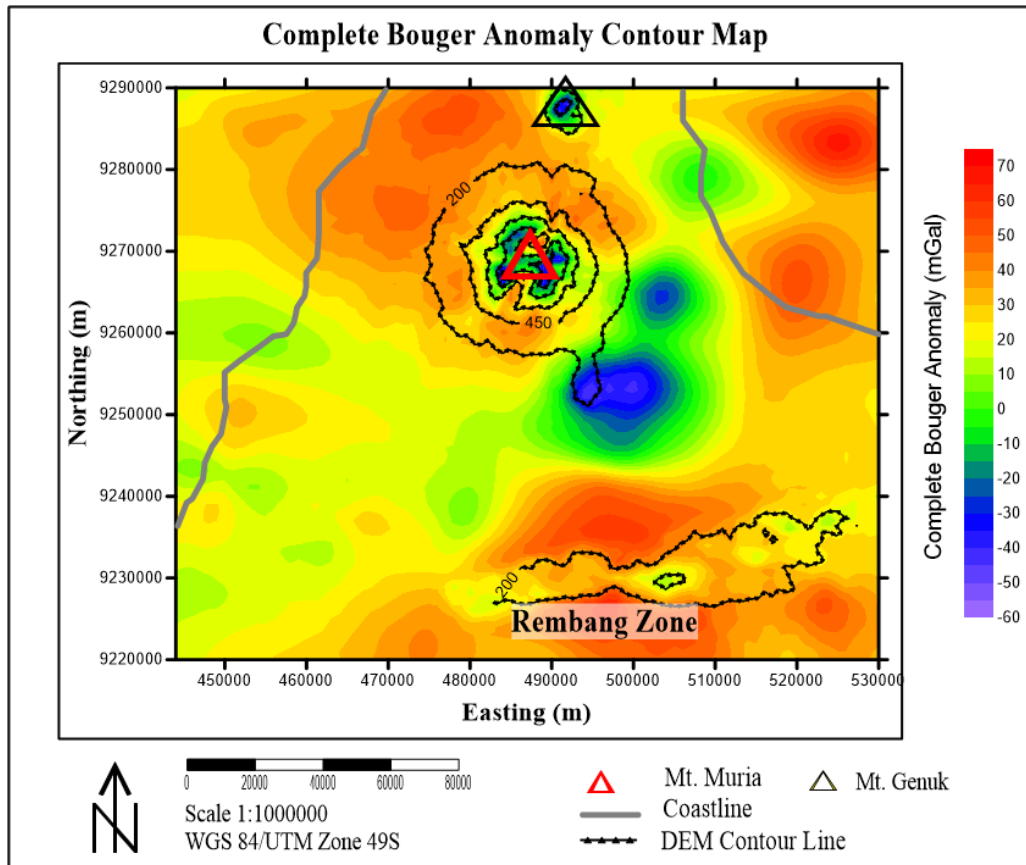
## RESULT
**Complete Bouger Anomaly**



**Figure 2. Complete bouger anomaly map**

CBA resulting from a series of FAA data reductions is shown in Figure 2. The CBA values range from -60 to 70 mGal. The red color on the contour map indicates high CBA values (30 to 70 mGal), found in the northern to northwestern areas of Mount Muria and the Rembang Fold Zone to the south. The green and yellow colors represent moderate anomalies (-10 to 30 mGal), distributed in the area between Mount Muria and the Rembang Fold Zone. The blue color indicates low anomalies (-60 to -10 mGal), found at the

summit of Mount Muria, Mount Genuk, and around the Patiayam Dome.

## Regional and Residual Anomaly

The separation of the CBA was performed using the upward continuation method and wavelet transform. Upward continuation was applied at an altitude of 15,000 meters, where the regional contours became smooth, and the residual contours highlighted shallow anomaly sources. The wavelet transform was conducted by applying a signal denoising function based on a threshold. Figures 2(a) and 2(b) show the results of anomaly separation using the upward continuation method, while Figures 2(c) and 2(d) present the results of anomaly separation using the wavelet transform method. The obtained values for the regional anomaly range from 17 to 38 mGal, while the residual anomaly values range from -85 to 35 mGal. The regional results exhibit a similar response, where the low anomalies smoothly align in a southwest–northeast direction. Similarly, the residual anomalies reveal detailed shallow anomaly sources, including Mount Genuk in the north, Mount Muria in the center, and the Patiayam Dome in the southeast of Mount Muria.
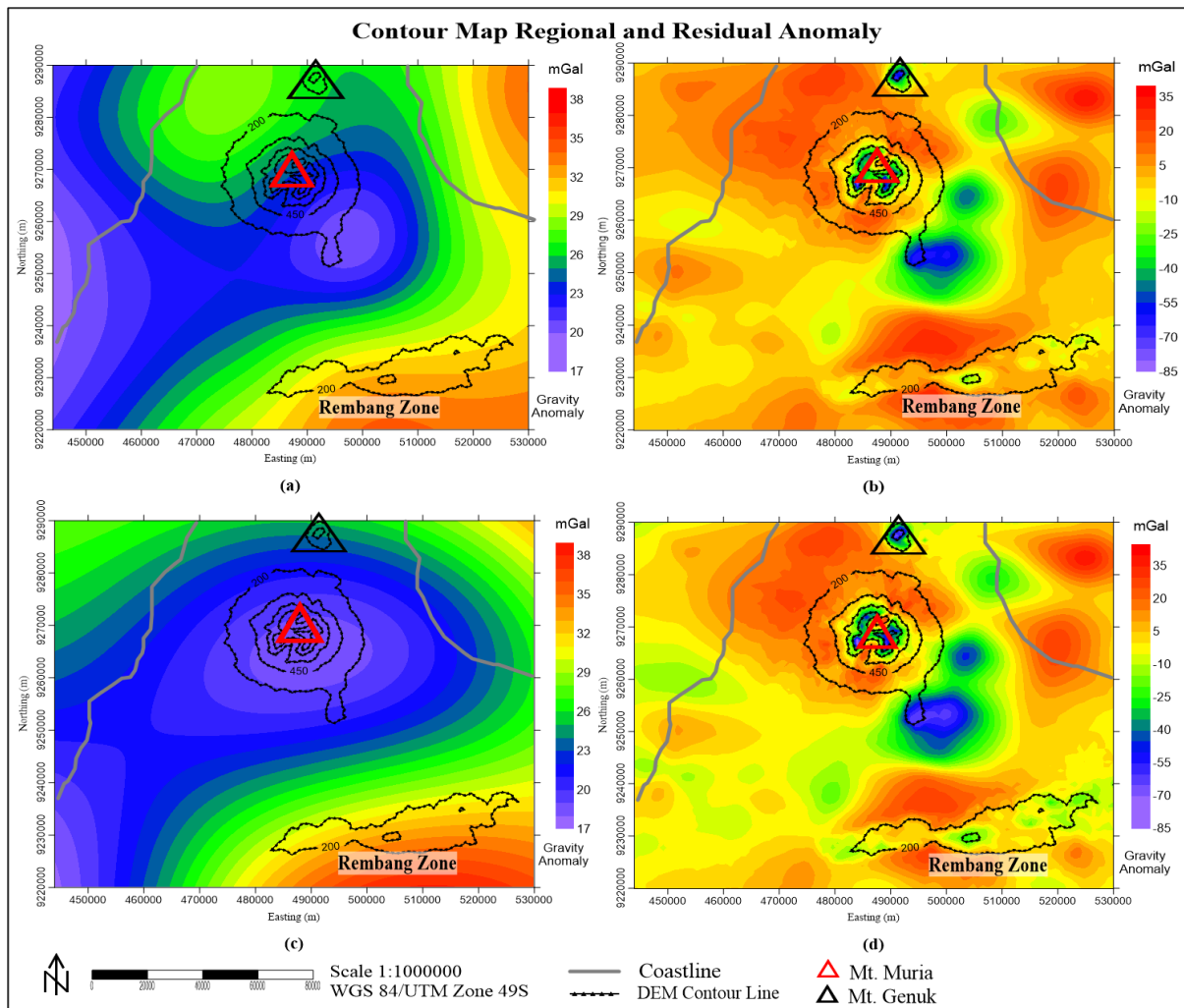


**Figure 3. Results of Anomaly Separation (a) Regional anomaly using the upward continuation method, (b) Residual anomaly using the upward continuation method, (c) Regional anomaly using the wavelet transform method, (d) Residual anomaly using the wavelet transform method**

## Correlation

Figure 4, the Pearson correlation graph, shows a positive correlation between the anomaly separation results obtained through the upward continuation and wavelet transform methods. The correlation results

are 0.81 for the regional anomaly and 0.98 for the residual anomaly, indicating a strong relationship between the two anomaly datasets. The correlation value for the regional anomaly is slightly lower than that of the residual anomaly due to the influence of a more complex regional trend. The high

correlation value in the residual anomaly suggests that both methods can be used for anomaly separation with minimal error. The more linear residual pattern indicates that the residual anomaly is more focused on local variations without interference from complex regional trends.
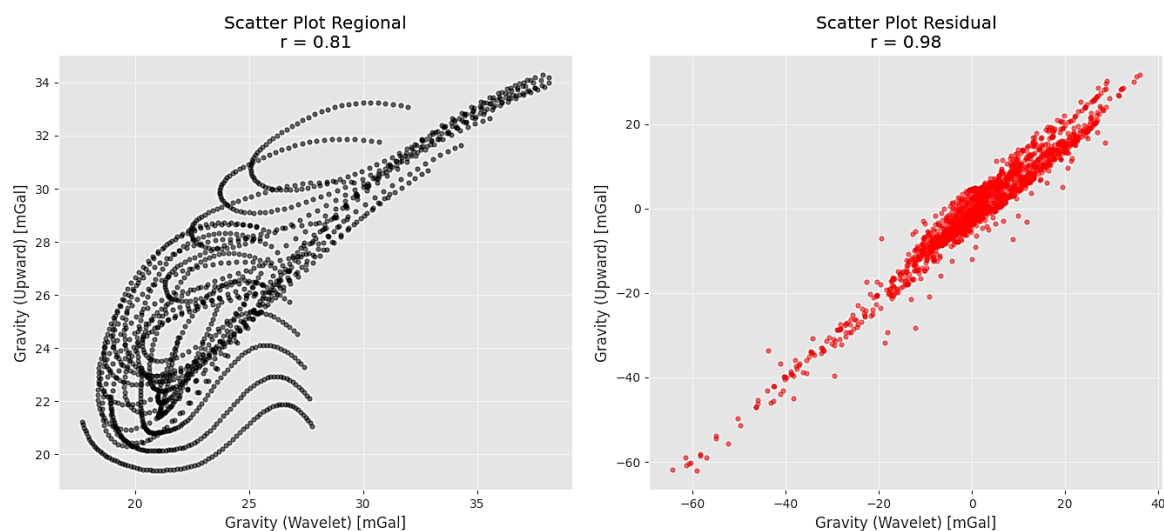


**Figure 4. Correlation graph of the upward continuation method and wavelet transform method**

## DISCUSSION

The CBA map in Figure 1 illustrates the distribution of gravity anomaly values across the Muria Peninsula. High CBA values in the northern region of Mount Muria are associated with rock structures of high density, which originate from volcanic rocks formed by the activity of Mount Genuk and Mount Muria. Moderate anomaly values between Mount Muria and the Rembang Fold Zone correspond to lowland areas filled with alluvial deposits. Low anomaly values are observed in Mount Muria and Mount Genuk, which are influenced by terrain correction effects that reduce gravity readings due to elevation. Additionally, the low gravity anomaly in Mount Muria is attributed to the presence of a caldera-shaped basin at the mountain's peak, while its slopes are surrounded by Maar Formations. Mount Genuk exhibits a low anomaly due to the presence of the Bulu Formation.

The regional and residual anomaly contour maps are shown in Figure 2, revealing variations in subsurface density models. The regional anomaly, with a range of 17 to 39

mGal, features smooth contours, indicating the presence of deeper anomaly sources. The residual anomaly, ranging from -85 to 35 mGal, has highly varied contours, suggesting shallow subsurface anomaly sources. Both regional and residual contours exhibit the same trends in the results obtained from upward continuation and wavelet transform methods. Therefore, both methods can be utilized for gravity data analysis.

The regional anomaly map reveals similar contour trends at several locations. Notably, in the southern part of the study area, which geologically belongs to the Rembang Fold Zone, this region is known for tectonic folding accumulation that has occurred since the Pliocene epoch, resulting in relatively high anomalies ranging from 29 to 30 mGal [27]. The smooth blue contours indicating low anomalies dominate the regional anomaly results. A slight difference between the two methods is observed, where the upward continuation results form a relatively high closure (green-colored) southwest of Mount Genuk. In contrast, the wavelet transforms results display a low anomaly

trend forming a closure extending to Mount Genuk. This suggests that the regional wavelet transform results better represent subsurface anomaly conditions, aligning with previous studies that indicate Mount Genuk and Mount Muria are connected through an underground magma channel [28].

The residual anomaly results provide more detailed information in specific areas such as Mount Muria, Mount Genuk, and the Rembang Fold Zone. The residual anomaly values from the upward continuation method range from -62 to -40 mGal in Mount Muria, -61 to -16 mGal in Mount Genuk, and -3 to 5 mGal in the Rembang Fold Zone. Meanwhile, the wavelet transforms residual anomaly values range from -72 to -20 mGal in Mount Muria, -63 to -18 mGal in Mount Genuk, and -14 to 6 mGal in the Rembang Fold Zone. The wavelet transforms results for Mount Muria provide a more detailed depiction of the volcanic peak structure, where a sharp, very low anomaly at the mountain's center indicates the presence of a caldera and maar formations [29,30]. Similarly, in Mount Genuk, the significant anomaly range observed in the wavelet transform results suggests the presence of volcanic rocks and the Bulu Formation [28]. In the Rembang Fold Zone, the wavelet transforms residual anomaly results reveal more detailed geological structures, capturing an east-west trending lineament. This lineament indicates the presence of a local fault [31].

The regional and residual results from the wavelet transform method show a broader range of values than those from the upward continuation method. This comparison indicates that anomaly separation using the wavelet transform produces sharper results than upward continuation. This is because wavelet anomaly separation employs a multiresolutional decomposition function, allowing for anomaly separation at various scales without sacrificing spatial resolution. In contrast, upward continuation smooths the data, sometimes causing the loss of shallow anomaly details. However, overall, both methods exhibit compatibility, as illustrated in Figure 4, where the correlation values approach 1.

## CONCLUSION

The upward continuation and wavelet transform methods produce the same trend, with a value range of 17 to 38 mGal for the regional anomaly and -85 to 35 mGal for the residual anomaly. This study provides a new perspective, showing that the wavelet transforms method yields sharper regional and residual anomalies compared to the upward continuation method. The sharpness of the wavelet transform results is evident in both regional and residual anomalies, where a broader value range is observed at several points, such as Mount Muria, Mount Genuk, and the Rembang Fold Zone. The regional anomaly from the wavelet transform method can indicate a possible connection between the magma pathways of Mount Genuk and Mount Muria. The residual anomalies in Mount Muria, Mount Genuk, and the Rembang Fold Zone also provide detailed results, revealing geological structures such as calderas, maars, and local faults.

## REFERENCES

1. Maithya J, Fujimitsu Y, Nishijima J. Analysis of gravity data to delineate structural features controlling the Eburru geothermal system in Kenya. Geothermics. 2020; 2(85):101795.
2. Lo YT, Ching KE, Yen HY, Chen SC. Bouguer gravity anomalies and the three-dimensional density structure of a thick mudstone area: A case study of southwestern Taiwan. Tectonophysics. 2023; 24(848): 229730.
3. Steenland NC. Gravity and aeromagnetic exploration in the paradox basin. Geophysics. 1962; 27(1):73–89.
4. Rosenbach O. A contribution to the computation of the "second derivative" from

gravity data. Geophysics. 1953 ;18(4):894–907.

5.  Vasanthi A, Santosh M. Overview of regional gravity field computation models and application of a novel method in imaging the lithospheric architecture and destruction of the North China Craton. Earth-Science Reviews. 2021; 215:103548.

6.  Bramanto B, Prijatna K, Pahlevi AM, et al. Determination of gravity anomalies in Java, Indonesia, from airborne gravity survey. Terrestrial Atmospheric and Oceanic Sciences. 2021; 32(2).

7.  Indrawati PI, Indriana RD, Nurwidyanto MI. Comparative Study on Separation of Regional and Residual Magnetic Anomalies Using the Upward Continuation, Moving Average, and Polynomial. Journal of Physics and Its Applications. 2020; 2(2):90–3.

8.  Griffin WL, O'Reilly SY, Natapov LM, et al. The evolution of lithospheric mantle beneath the Kalahari Craton and its margins. Lithos . 2003; 71(2):215–41.

9.  Mallick K, Vasanthi A, Sharma KK. Bouguer Gravity Regional and Residual Separation: Application to Geology and Environment. Springer eBooks. 2012.

10. Feng X, Zong X, Wang X, et al. Moho depth variations of Zealandia from gravity data inversion and implications for continental breakup. Tectonophysics. 2025; 230643.

11. Xu W, Yao C, Yin X, et al. Crustal configuration beneath the Santos and Campos Basins, southeastern Brazil: A refined Moho depth model based on gravity and seismic data in spherical coordinates. Physics and Chemistry of the Earth Parts A/B/C . 2024; 135:103661.

12. Teknik V. The improved Moho depth imaging in the arabia-eurasia collision zone: A machine learning approach integrating seismic observations and satellite gravity data. Tectonophysics. 2024; 893:230553.

13. Panthi J, Johnson CD, Pradhanang SM, et al. Delineating bedrock topography with geophysical techniques: An implication for groundwater mapping. Catena. 2023; 230:107258.

14. Zhang C, Yang J, Yang F, et al. Identification of lithological discontinuities and preliminary exploration of material sources in typical mountain soils of the southern margin of the Qinghai-Tibet Plateau. Catena. 2025; 251:108819.

15. Wu Y, Liang F, Yan J, et al. Analysis of regional and residual gravity disturbance of major fault belts in the Tarim Basin, Western China. Remote Sensing. 2022; 14(16):3948.

16. Lucero SEV, Almaraz F, Prezzi CB, et al. Tectonic structures of SW margin of Gondwana from gravity and magnetic anomalies of the Río de la Plata area and their correlation with the Beattie magnetic Anomaly in South Africa. Tectonophysics. 2024; 230571.

17. Indriyani PD, Indriana RD, Sabri LOM. Semarang subsurface model using airborne gravity data. International Journal of Research and Review. 2023; 10(9):271–80.

18. Kebede H, Alemu A, Nedaw D. Mapping geologic structures from Gravity and Digital Elevation Models in the Ziway-Shala Lakes basin; central Main Ethiopian rift. Heliyon . 2021; 7(12):e08604.

19. Indriana RD, Brotopuspito KS, Setiawan A, et al. A Comparison Of Gravity Filtering Methods Using Wavelet Transformation And Moving Average (A Study Case Of Pre And Post Eruption Of Merapi In 2010 Yogyakarta, Indonesia). Journal of Applied Geology and Geophysics. 2017; 6(3):44–57.

20. Hwang C, Hsiao YS, Shih HC. Data reduction in scalar airborne gravimetry: Theory, software and case study in Taiwan. Computers & Geosciences. 2006; 32(10):1573–84.

21. Fairhead J D, Cooper G R J, Sander S. Advances in Airborne Gravity and Magnetics. Airborne Geophysics. In: Tschirhart and Thomas MD. Proceedings of Exploration 17: Sixth Decennial International Conference on Mineral Exploration; Airborne Geophysics; 2016. p. 113-127.

22. Jacobsen B H. Case for upward continuation as a standar separation filter for potential field maps. Geophysics. 1987; 52:1138–48.

23. Kebede H, Alemu A, Fisseha S. Upward continuation and polynomial trend analysis as a gravity data decomposition, case study at Ziway-Shala basin, central Main Ethiopian rift. Heliyon. 2020; 6(1): e03292.

24. Mallat SG, Peyré G. A Wavelet tour of Signal Processing: The Sparse Way. Elsevier eBooks. 2008.

25. Geetha K, Hota MK, Karras DA. A novel approach for seismic signal denoising using optimized discrete wavelet transform via honey badger optimization algorithm.

Journal of Applied Geophysics. 2023; 219:105236.

26. Karthikeyan P, Murugappan M, Yaacob S. ECG signal denoising using Wavelet thresholding techniques in human stress assessment. International Journal on Electrical Engineering and Informatics. 2012; 4(2):306–19.

27. Husein S, Titisari AD, Freski YR, Utama PP. Panduan Ekskursi Geologi Regional 2016 - Jawa Timur bagian barat, Indonesia. Yogyakarta: Universitas Gadjah Mada; 2016.

28. Panjaitan S, Subagio S. Indikasi fenomena struktur geologi bawah permukaan daerah rencana tapak pembangkit listrik tenaga nuklir Gunung Api Genuk dan sekitarnya, Jepara, Jawa Tengah. Jurnal Geologi Dan Sumberdaya Mineral. 2009; 19(1):47–61

29. Indriana RD. Distribution of subsurface anomalies in the Muria Peninsula and depth analysis with euler deconvolution. International Journal of Physical Sciences and Engineering. 2019; 3(3):21–30.

30. Bronto S, Mulyaningsih S. Gunung api maar di Semenanjung Muria. Indonesian Journal on Geoscience. 2007; 2(1):43–54.

31. Navalia AI, Realita A, Prastowo T. Analisis anomali gravitasi Gunung Semeru pasca erupsi 4 Desember 2021. Inovasi Fisika Indonesia. 2023; 12(1):63–74.

******